



Article

Characterization and Computation of Yb/TiO₂ and Its Photocatalytic Degradation with Benzohydroxamic Acid

Xianping Luo ^{1,2,3}, Sipin Zhu ^{1,3}, Junyu Wang ^{1,3}, Chunying Wang ^{1,2,3,*}  and Min Wu ²

¹ Faculty of Resource and Environmental Engineering, Jiangxi University of Science and Technology, Ganzhou 341000, China; lxp9491@163.com (X.L.); Zhusipin926@163.com (S.Z.); Wangjunyu1025@163.com (J.W.)

² Post-Doctoral Scientific Research Workstation of Western Mining Co. Ltd., Xining 810001, China; wumin5836@163.com

³ Jiangxi Key Laboratory of Mining and Metallurgy Environmental Pollution Control, Ganzhou 341000, China

* Correspondence: cywang@jxust.edu.cn; Tel.: +86-797-831-2706

Received: 31 October 2017; Accepted: 20 November 2017; Published: 28 November 2017

Abstract: Yb-doped TiO₂ (Yb/TiO₂) compositions were synthesized by sol-gel method, and the prepared materials were characterized by X-ray Diffraction (XRD), X-ray photoelectron spectroscopy (XPS), UV-visible diffuse-reflectance spectrum (UV-Vis DRS), transmission electron microscope (TEM) and high resolution transmission electron microscope (HRTEM), energy dispersive spectrometer (EDS), and N₂ adsorption. A beneficiation reagent of benzohydroxamic acid (BHA) was used to test the photocatalytic activity of Yb/TiO₂. The characterizations indicate that the doping of Yb could inhibit the crystal growth of TiO₂, enhance the specific surface area, increase the binding energy of Ti2p, and also slightly expand the adsorption ranges to visible light. Furthermore, the computation of band structure also indicates that Yb-doped TiO₂ could make the forbidden band narrower than pure anatase TiO₂, which presents a red shift in the absorption spectrum. As a result of the photodegradation experiment on BHA, Yb/TiO₂ (0.50% in mass) sintered at 450 °C displayed the highest catalytic activity for BHA when compared with pure TiO₂ or other doped Yb/TiO₂ compositions, and more than 89.2% of the total organic carbon was removed after 120 min. Almost all anions, including Cl⁻, HCO₃⁻, NO₃⁻, and SO₄²⁻, inhibited the degradation of BHA by Yb/TiO₂, and their inhibition effects followed the order of HCO₃⁻ > NO₃⁻ > SO₄²⁻ > Cl⁻. Cations of Na⁺, K⁺, Ca²⁺, and Mg²⁺ displayed a slight suppressing effect due to the impact of Cl⁻ coexisting in the solution. In addition, Yb/TiO₂ maintained a high photocatalytic ability with respect to BHA after four runs. It is hypothesized that ·OH is one of the main species involved in the photodegradation of BHA, and the mutual transformation of Yb³⁺ and Yb²⁺ could promote the separation of electron-hole pairs.

Keywords: benzohydroxamic acid; characterization; computation; rare earth; Yb; active species

1. Introduction

TiO₂ is considered to be one of the most promising and widely used semiconductor photocatalyst materials, primarily due to its chemical stability, unique optical properties, nontoxicity, strong oxidizing power, and low cost [1]. However, the largest obstacles to its use are the wide band gap (3.2 eV) and the easy recombination of photogenerated electron-hole pairs, which limit the use of solar light and reduce photon efficiency [2]. Therefore, improvement of photocatalytic activity has been a core topic in photocatalysis research field in recent years. Doping with metal ions in the TiO₂ lattice has been proven to be an efficient way to enhance photocatalytic activity [3,4]. Research has shown that the doping of rare earth ions can effectively improve the photocatalytic activity of TiO₂ [5–7]. Rare earth elements

have the electronic structure of 4f, which exists at the ground and excited states. When photo-excited electrons were captured, Re^{3+} changed into Re^{2+} . After that, Re^{2+} was able to react with O_2 adsorbed on the surface of catalysts to produce Re^{3+} and O_2^- . Thus the doping of rare earth could reduce the recombination of photogenerated electron-hole pairs [8,9].

Benzohydroxamic acid (BHA) is most widely used as a collector in the flotation industry at present. However, the dosage of BHA is usually more than 1 kg/t ore [10]. The discharge of mineral-processing wastewater containing BHA from concentrator plants can increase COD content and result in eutrophication because of the benzene ring structure and accumulation of N elements [11]. Besides, the degradation process of BHA is complex, and it can remain for several years or even longer in water. Finally, BHA is be harmful to the water environment and needs to be treated. The biodegradation method has been used to treat BHA [12]. However, five or more days were needed to obtain a removal efficiency of 85% under the conditions of additional nutrition. Our previous study indicated that La/TiO₂ possessed high activity with respect to BHA [13]. However, the products of BHA and the oxidation mechanisms were not discussed in the previous study.

In this study, Yb-doped TiO₂ (Yb/TiO₂) composites were synthesized by the sol-gel method, and their physicochemical properties were characterized by XRD, X-ray photoelectron spectroscopy (XPS), UV-visible diffuse-reflectance spectrum (UV-Vis DRS), N₂ adsorption, and TEM. Besides, the band structure and density of states were calculated by computer. As a target pollutant, BHA was used to test the photocatalytic activity of the Yb/TiO₂ composition. The effects of Yb-doping amount, calcination temperature, common anions and cations in the photodegradation of BHA, and the degradation mechanism of BHA were investigated, and the reuse of doped catalyst was also investigated.

2. Materials and Methods

2.1. Materials

Tetra butyl titanite and Ytterbium nitrate were bought from the National Medicine Group Chemical Reagent Co. Ltd., Shanghai, China. Anhydrous ethanol, KI, ammonium oxalate, acetic acid, and isopropanol were obtained from the Tianjin Damao Chemical Reagent Factory, Tianjin, China. Benzohydroxamic acid was bought from Shanghai EKEAR Bio@Tech Co. Ltd., Shanghai, China. All the reagents were of analytical grade and used as received without any purification.

2.2. Synthesis of Yb/TiO₂

Pure TiO₂ and Yb/TiO₂ catalysts were synthesized by sol-gel method [13–15]. The detailed prepared processes are as follows. First, 10 mL of tetra butyl titanite were dissolved in 15 mL anhydrous ethanol to get a mixture solution noted as solution A, and solution A was stirred for 30 min; second, solution B was prepared using 2 mL acetic acid, 10 mL ethanol, 2 mL deionized water, and Ytterbium nitrate in the required stoichiometry (the doping ratios of Yb were set to 0%, 0.10%, 0.30%, 0.50%, 0.70%, and 1% according to the mass fraction of Yb to TiO₂.); third, the transparent homogeneous sol was gained by adding dropwise solution B to the solution A under acute and continuous agitation; fourth, the aerogel was formed after ageing at room temperature for 2 days and then dried at 90 °C; and finally, pure TiO₂ and Yb/TiO₂ were achieved after calcining (400 °C, 450 °C and 500 °C) of the aerogel in muffle furnace under air atmospheres.

2.3. Characterization

The XRD patterns were carried out with an X-ray diffractometer (Rigaku Miniflex, Rigaku Corporation, Tokyo, Japan) using monochromatized Cu K α radiation ($\lambda = 0.15418$ nm). The element constitutions were analyzed by X-ray photoelectron spectroscopy (XPS) on a Thermo-type multi-function imaging electronic spectrometer (ESCALAB 250XI, Thermo Fisher Scientific, Waltham, MA, USA). The property of light absorption of materials was studied using a UV-Vis spectrophotometer

(UV-2550, Shimadzu Scientific Instruments, Tokyo, Japan). Nitrogen adsorption–desorption isotherms were recorded by adsorption apparatus (ASAP 2460, Micromeritics Instrument Corporation, Norcross, GA, USA) at liquid nitrogen temperature ($-196\text{ }^{\circ}\text{C}$) and the specific surface area and average pore size of TiO_2 or La/TiO_2 were measured by the Brunauer-Emmett-Teller (BET) method. Morphology of catalysts was observed by a Tecnai transmission electron microscope (FEI G2-20, Hillsboro, AL, USA).

2.4. Photocatalytic Degradation Tests

Band structure and partial density of states (PDOS) were calculated based on the density functional theory (DFT) implemented in the Cambridge Serial Total Energy Package (CASTEP, MS2016) [16].

The general gradient approximation (GGA) exchange–correlational functional was used and treated with Perdew-Burke-Ernzerhof (PBE) scheme. Geometry optimization was adopted. The detailed calculation conditions are as follows: convergence of energy change per atom at 5×10^{-6} eV, residual force at $0.01\text{ eV}/\text{\AA}$, stress at 0.02 GPa , and displacement of atoms at 0.0005 \AA . The Broyden-Fletcher-Goldfarb-Shanno (BFGS) algorithm was used in the optimization. The self-consistent field tolerance was 1.0×10^{-7} eV/atom. The FFT (Fast Fourier Transformation) grid of the basis was $50 \times 50 \times 64$ and the kinetic energy cutoff for the plane-waves basis was 400 eV . A $3 \times 3 \times 3$ k-point and the ultrasoft pseudopotential were applied in above calculation. The electronic configurations considered are $3s^23p^63d^24s^2$ (Ti), $2s^22p^4$ (O), and $4f^{14}5s^25p^66s^2$ (Yb) for TiO_2 (unit cell) and TiO_2 (Yb, $2 \times 2 \times 1$ supercell) (Figure S1).

2.5. Photocatalytic Degradation Tests

The photocatalytic tests were carried out in a light chemical reaction apparatus from XPA-7 (Xujiang Electromechanical Factory, Nanjing, China). In order to ensure the adsorption-desorption equilibrium of BHA in photocatalysts, the reaction solution was magnetically stirred for 30 min without irradiation. Then, a 300 W mercury light was turned on. Approximately 5 mL of suspension solution was taken at given time intervals and the supernatant was tested by UV-Vis spectrophotometry at 229 nm after being centrifuged. The removal efficiency (R) was calculated by Equation (1), where C_0 (mg/L) is the initial concentration of BHA and C_t (mg/L) is the concentration at reaction time t (min).

$$R = (C_0 - C_t) \times 100\%/C_0 \quad (1)$$

The total organic carbon (TOC) was detected by the total organic carbon analyzer (Elementar Analysensysteme GmbH, Langenselbold, Germany). Ionic chromatography (ICS-1100, Thermo Fisher Scientific, Waltham, MA, USA) was used to detect the existence and concentration of NO_3^- and NO_2^- in degradation products. In addition, the effects of common inorganic cations and anions (Na^+ , K^+ , Ca^{2+} , Mg^{2+} , Cl^- , HCO_3^- , NO_3^- , SO_4^{2-}) in waters on the photodegradation of BHA were investigated.

3. Results and Discussion

3.1. Characterization

3.1.1. XRD

Figure 1 shows the XRD patterns of prepared TiO_2 doped with different amounts of Yb. It is observed that major peaks at 2θ values of 25.21° , 37.53° , 47.87° , 53.53° , 54.86° , 62.37° , 68.30° , 70.03° and 74.63° corresponded to the diffraction planes (101), (004), (200), (105), (211), (204), (116), (220) and (215), respectively, of anatase TiO_2 . Hence, Yb/TiO_2 retains the crystal phase of TiO_2 . However, the diffraction peak of pure TiO_2 is relatively narrow compared with Yb/TiO_2 . The higher the Yb doping amount, the broader of the peaks, and the lower of the intensity [17]. In other words, the doping of Yb slowed down the growth of TiO_2 nanoparticles, changed the structure of TiO_2 particles, and increased the diffusion barrier of grain. Thus, doping of Yb led to a systematic decrease in grain.

The Scherrer formula [18] is used to calculate the crystallite sizes in the form of Equation (2):

$$D = 0.89\lambda / \beta \cos\theta \quad (2)$$

where D is crystallite size, λ (nm) is wavelength of X-ray, β (rad) is full width at half maximum of the peak, and θ (rad) is the angle of diffraction. As a result, the crystallite sizes of pure TiO_2 and 0.50% Yb/TiO_2 are 19 nm and 13 nm, respectively. It is proposed that the doping of Yb could inhibit the crystal growth of TiO_2 because of quantum size. Liu reported that the RE-doped TiO_2 nanocrystals almost had the capacity to enhance photocatalytic activity due to the quantum size effect of prepared $\text{RE}^{3+}/\text{TiO}_2$ [19].

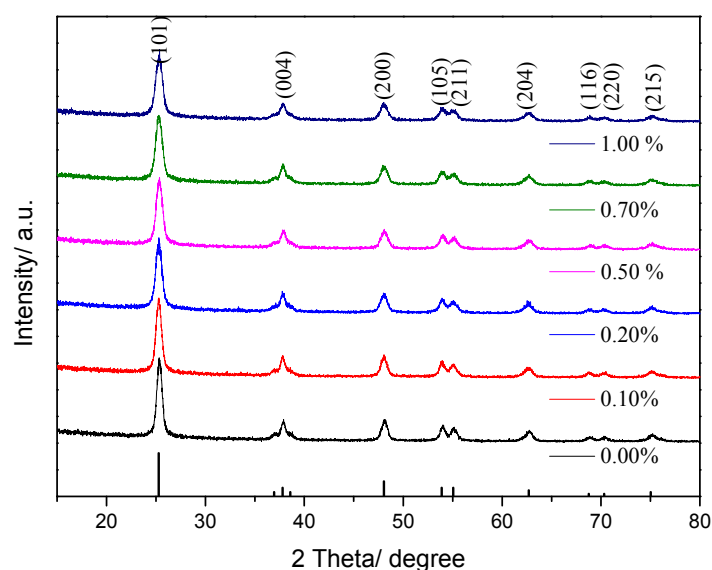


Figure 1. XRD (X-ray Diffraction) patterns of Yb/TiO_2 with different doping amounts, calcined at 450 °C.

3.1.2. XPS

As seen from Figure 2a of the survey spectrum, there are relative peaks corresponding to the elements Ti and O that come from the prepared TiO_2 . Figure 2b shows the spectra ranges of doped Yb. However, similar to pure TiO_2 , the characteristic peaks of Yb^{3+} and Yb^{2+} are not detected near 182.1 eV and 190.9 eV, which indicates that the content of Yb on the surface of the catalyst was very low.

The two peaks of $\text{Ti}2p$ for pure TiO_2 and Yb/TiO_2 were composed of $\text{Ti}2p_{1/2}$ and $\text{Ti}2p_{3/2}$, which indicates the existence of a +4 valence for Ti atom. The Ti peaks of pure TiO_2 are at 464.52 eV and 458.82 eV, while the peaks are at 464.75 eV and 459.06 eV for Yb/TiO_2 . As seen from Figure 2e,f, the characteristic peak of $\text{O}1s$ was wide and asymmetric, and was fitted into two kinds of chemical states by curve fitting: crystal lattice oxygen (lower) and hydroxyl oxygen (higher) [1]. The fitted peak of $\text{O}1s$ located at 530.07 eV was for lattice oxygen, while the peak at 530.63 eV corresponded to hydroxyl oxygen on the surface of pure TiO_2 . After doping, $\text{O}1s$ spectrum peaks slightly decreased to 529.87 eV and 530.49 eV for lattice oxygen and hydroxyl oxygen, respectively. As discussed above, the binding energy of $\text{Ti}2p$ increased, while the binding energy of $\text{O}1s$ decreased for Yb/TiO_2 compared pure TiO_2 . This might be due to the fact that Yb and Ti elements combine to form new chemical bonds of $\text{Ti}-\text{Yb}$ [20], which leads to a decrease of +4 valences for Ti in Yb/TiO_2 .

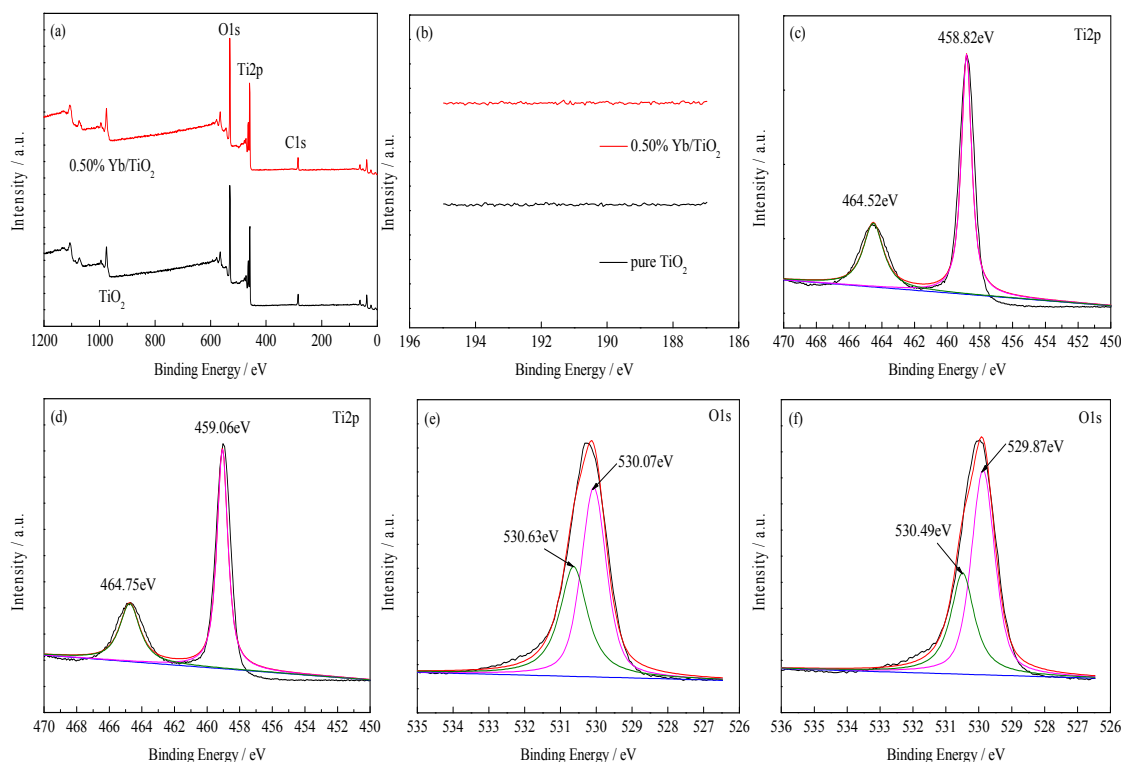


Figure 2. X-ray photoelectron spectroscopy (XPS) spectra. Survey spectra (a), Yb3d (b), Ti2p and O1s of pure TiO₂ (c,e), and Ti2p and O1s of Yb/TiO₂ (d,f), respectively. Different color mean different curves in Figure 2c–f. Black, original curve; red, fitted curve; green, hydroxyl oxygen curve; pink, crystal lattice oxygen curve; blue, background.

3.1.3. UV-Vis DRS

The UV-Vis DRS curves of pure TiO₂ and 0.50% Yb/TiO₂ are shown in Figure 3. There is a slight red shift of Yb/TiO₂ compared with pure TiO₂, which was supported by the band gap energy (E_g) calculated by Formula (3) as follows [21]:

$$ahv = A (hv - E_g)^{n/2} \quad (3)$$

where v , h , A and a represent the light frequency, Planck's constant, a constant, and the absorption coefficient, respectively. The value of n is determined by the semiconductor's optical transition type: for indirect transition, $n = 4$; and for direct transition, $n = 1$. By calculation, the E_g values for pure TiO₂ and 0.50% Yb/TiO₂ were 3.20 eV and 3.16 eV, respectively. The red shift could be attributed to the charge-transfer transition between the 4f electrons of Yb and the conduction or valence band of TiO₂ [22]. As discussed above, the doping of Yb can narrow the band gap of TiO₂ and reduce the band gap energy, which is important to slow down the recombination rate of the electron-hole pairs and ultimately augment the photocatalytic activity [23].

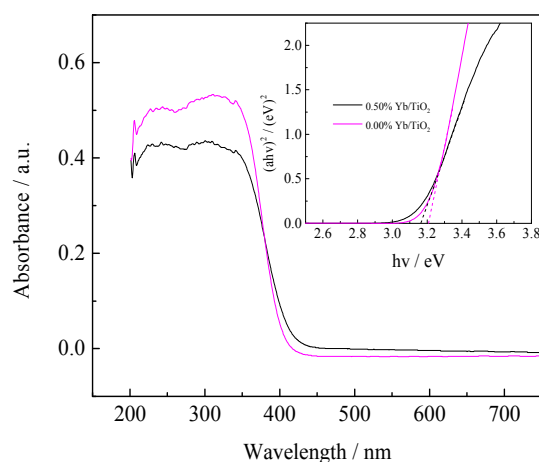


Figure 3. UV-Vis DRS spectra of pure TiO_2 and 0.50% Yb/TiO_2 . UV-Vis DRS: UV-visible diffuse-reflectance spectrum.

3.1.4. S_{BET} and Porosity Analysis

The N_2 adsorption-desorption isotherms in Figure 4 indicate the typical Langmuir IV isotherm with a hysteresis loop, which indicates the mesoporous structure of synthesized samples [24,25]. The hysteresis loops of pure TiO_2 and 0.50% Yb/TiO_2 are consistent with type H_2 that has uniform particle accumulation in the hole. The shape of the holes is considered to be an ink bottle-shaped channel of the small mouth and large cavity [26]. As shown in Figure 4a,b the distribution of pore size ranges from 2 nm to 10 nm. This is in the mesoporous range and is in accordance with what has been discussed above. Besides, the most probable pore size of pure TiO_2 was 9.01 nm, while it was 8.94 nm for 0.50% Yb/TiO_2 . The S_{BET} values were $87 \text{ m}^2/\text{g}$ and $114 \text{ m}^2/\text{g}$ for pure TiO_2 and 0.50% Yb/TiO_2 , respectively. Obviously, the S_{BET} of 0.50% Yb/TiO_2 is much larger than that of pure TiO_2 , which means the doped catalyst could have better adsorption ability than the undoped catalyst. The reason may be due to the linkage between the rare earth ions and titanium by an oxygen bridge, which could effectively enhance the specific surface area of TiO_2 [27]. Generally speaking, the larger the specific surface area, the more surface reaction sites. This is an advantage for the improvement of photocatalytic activity.

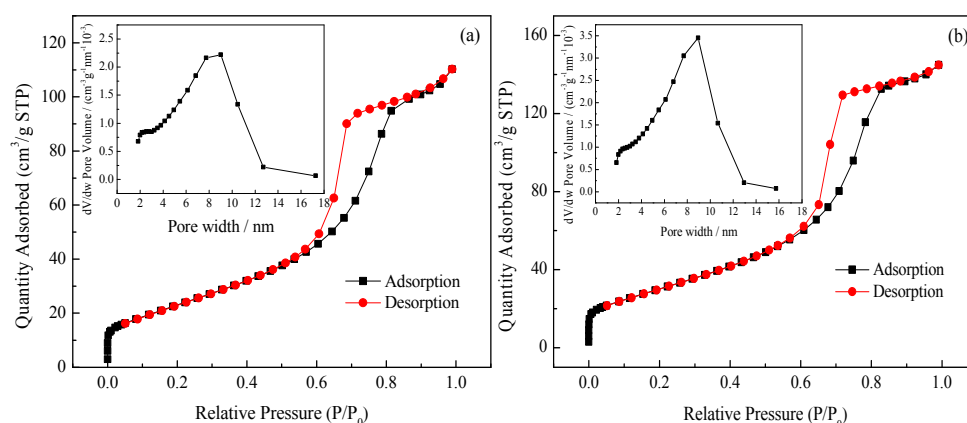


Figure 4. N_2 adsorption-desorption isotherms and pore size distributions (inset) of pure TiO_2 (a) and 0.50% Yb/TiO_2 (b).

3.1.5. Microstructure Analysis

The particle size of 0.50% Yb/TiO₂ is in the range of 10~15 nm as seen from Figure 5a, which is in accordance with the XRD calculation using the Scherrer formula. However, there is still a significant agglomeration for the doped catalyst due to the smaller particle size. The corresponding FFT pattern formed in Figure 5b shows that the Yb³⁺-doped TiO₂ is a polycrystalline structure. The compositions and elements of Yb/TiO₂ are further investigated with EDS (energy dispersive spectrometer): the detected doped amount of Yb was about 0.3%, which was lower than the experimental value of 0.5%, and element mapping indicated successful doping as shown in Figure S2.

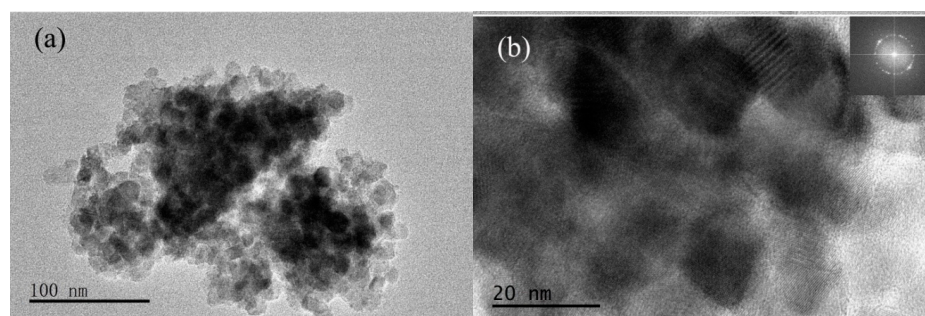


Figure 5. TEM (a) and HRTEM (b) images of 0.50% Yb/TiO₂. HRTEM: high resolution transmission electron microscope.

3.2. Photodegradation of Benzohydroxamic Acid

3.2.1. Effect of the Doped Amount

The photodegradation of BHA can be described by an apparent first-order equation with a simplified Langmuir-Hinshelwood model: $\ln(C_0/C_t) = kt$, where C_0 (mg/L) is the initial concentration of BHA, C_t (mg/L) is the concentration at reaction time t (min), and k (min^{-1}) is the apparent first-order rate constant. Table 1 indicates the linear relationship between $\ln(C_0/C_t)$ and t (min), confirming that the photodegradation reaction is indeed a first-order reaction. Besides, the rate constant of 0.50% Yb/TiO₂ was up to 0.0392 min^{-1} . Due to the fact that the radius of Ti⁴⁺ (0.068 nm) is much smaller than that of Yb³⁺ (0.115 nm), Ti⁴⁺ may enter the lattices of Yb³⁺ during synthesis, which might induce a great deal of lattice distortions and plenty of defects at/under the surface of Yb-doped TiO₂ nanoparticles [28]. The generated defects would decrease the recombination of electron-hole pairs. However, if the doped amount was continuously increased, this would produce defects, which would become the center of recombination again. Therefore, there exists an optimum doping ratio. It might be 0.5% in this study. As seen from Figure S3, 450 °C was the appropriate prepared temperature, and the following photodegradation experiments all used 0.50% Yb/TiO₂ calcined at 450 °C.

Table 1. Parameters of the first-order reaction kinetics.

Doped Ratio	R ²	k (min ⁻¹)
0%	0.9994	0.0339
0.1%	0.9979	0.0375
0.3%	0.9981	0.0372
0.5%	0.9967	0.0392
0.7%	0.9910	0.0335
1%	0.9990	0.0327

In addition to photoactivity, reusability is also an important characteristic of photocatalysts. Therefore, four cycling tests were performed to demonstrate the reusability of Yb/TiO₂ for

photodegradation of BHA. As shown in Figure S4, after four cycling tests, the degradation efficiency only reduced about 2% compared to the first run. Yb/TiO₂ retains photocatalytic activity on photodegradation of BHA, confirming potential reusability in practical applications.

3.2.2. Effect of Inorganic Ions

There are some common inorganic ions (Cl⁻, HCO₃⁻, NO₃⁻, SO₄²⁻, Na⁺, K⁺, Ca²⁺ and Mg²⁺ are taken into account) in natural water. Their existence might affect the removal efficiency of pollutants and Figure 6 illustrates the effects of these eight ions on the photodegradation of BHA by Yb/TiO₂.

As shown in Figure 6a, Cl⁻ has slight effect on the degradation of BHA. SO₄²⁻ can react with the valence band hole (h⁺) [29], and compete with BHA for the holes, reducing the degradation rate. However, generated h⁺ is not the main species involved in the photodegradation of BHA, as discussed later. Therefore, SO₄²⁻ also has little effect on the photodegradation. For NO₃⁻, Sørensen [30] indicated that NO₃⁻ could act as an “inner filter” and reduce the UV light intensity to the reaction solution. Therefore, addition of NO₃⁻ inhibited the removal efficiency of BHA in the reaction process. In addition, nitrate ions were produced as the reaction went on because of the existence of N-containing functional groups in the molecule of BHA. The excessive NO₃⁻ could be adsorbed on the catalyst and compete for the active sites on the catalyst surface with BHA. As discussed in a published paper [13], addition of HNO₃ would inhibit the photodegradation significantly, because of the existence of N-containing functional groups in molecular BHA. The detected result by ionic chromatography also manifested in the production of NO₃⁻ during the photodegradation of BHA. HCO₃⁻ could react with ·OH to produce carbonate radicals (HCO₃⁻ + ·OH → ·CO₃⁻ + H₂O) [31], which possess too weak an oxidizing ability to react with other pollutant molecules. In addition, the later discussion will demonstrate the strong ability of ·OH. Like NO₃⁻, HCO₃⁻ displayed significant inhibition effect on BHA photodegradation by Yb/TiO₂.

As shown in Figure 6b, the four metal ions (Na⁺, K⁺, Ca²⁺, and Mg²⁺) displayed inhibition effects on BHA removal. This is attributed to the effect of Cl⁻ ions co-present in the solution, because the four metal ions were used in their chloride salts. As described above, Cl⁻ ions inhibit photodegradation slightly [32].

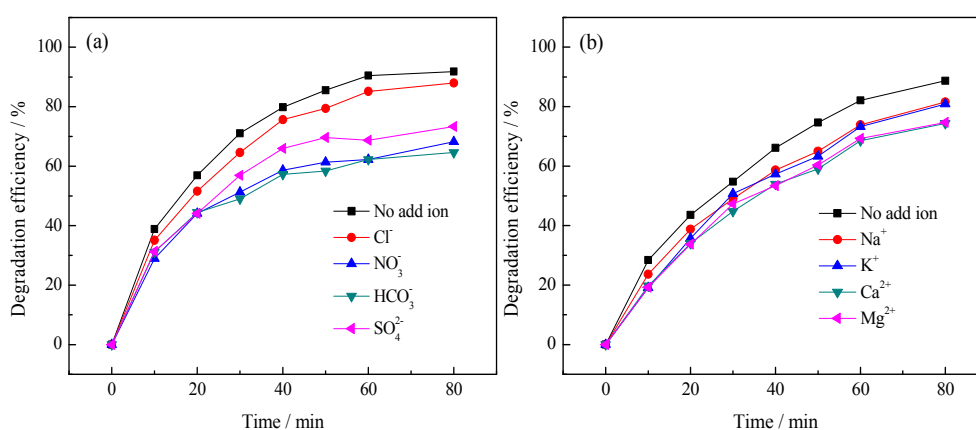


Figure 6. Effect of inorganic anions (a) and cations (b) on the degradation of benzohydroxamic acid by Yb/TiO₂. The benzohydroxamic acid (BHA) concentration was 30 mg/L, the catalyst dosage was 0.3 g/L, and the concentrations of cation ions and anion ions were 5 mmol/L.

3.3. Mechanism Analysis

As is well known, active species such as h⁺ and ·OH might play important roles in the photocatalytic oxidation process. In order to reveal the possible photocatalytic mechanism of Yb/TiO₂ on BHA, the active species trapping experiment were carried out (Figure 7). Isopropanol and ammonium oxalate were used as the scavengers of ·OH and h⁺, respectively [33,34]; KI could not

only capture $\cdot\text{OH}$, but also h^+ [33]. As a result, the presence of ammonium oxalate (an h^+ scavenger) almost had no influence on the rate of BHA degradation, while the addition of isopropanol (an $\cdot\text{OH}$ scavenger) and KI (an $\cdot\text{OH}$ and h^+ scavenger) inhibited the photodegradation of BHA by Yb/TiO₂. The results suggest that $\cdot\text{OH}$ is one of the main species involved in the photodegradation of BHA.

UV-Vis absorbance spectra of BHA solutions at different irradiation times were performed to investigate the degradation processes of the beneficiation reagent. As shown in Figure 8, the maximum adsorption intensity of BHA is gradually decreasing with the irradiation time. After 120 min, the light adsorption curve almost becomes a horizontal line, indicating the complete decomposition of BHA by Yb/TiO₂ during the degradation processes. Besides, the mineralization rate is also an important indicator to measure the degree of degradation of organic pollutants. The removal efficiency of TOC reached 89.2% by 0.50% Yb/TiO₂ after 120 min of irradiation, while the removal efficiency was 69.5% by pure TiO₂ (Figure S5). As such, TiO₂ doped with Yb indeed thoroughly promotes photodegradation.

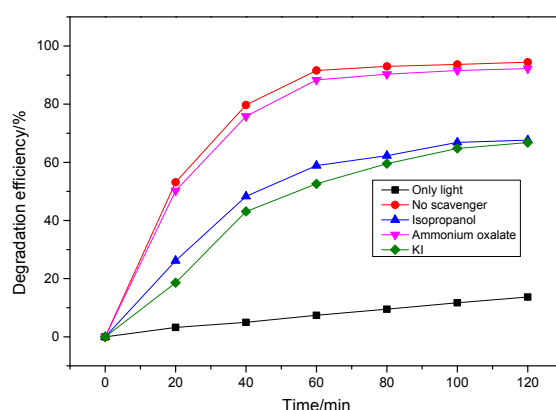


Figure 7. The effect of a series of scavengers on the photocatalytic efficiency of 0.50% Yb/TiO₂. The BHA concentration was 30 mg/L, the catalyst dosage was 0.5 g/L, and the concentration of all scavengers was 10 mmol/L.

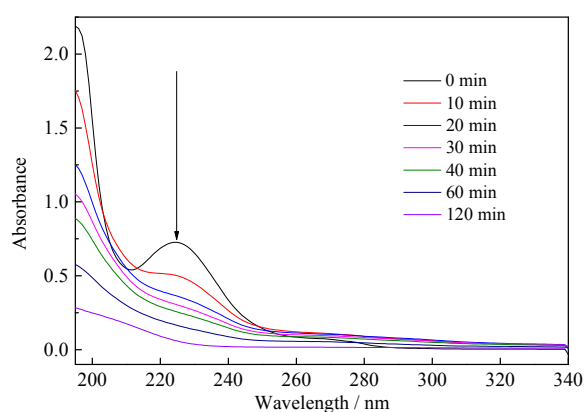


Figure 8. UV-Vis absorbance spectra of benzohydroxamic acid solution at different irradiation times.

The TOC data explain the conversion of the C element from organic chemicals to inorganic matter. In addition to the C element, there is also N-containing functional group (amino group) in the molecule of BHA. Both NO₃⁻ and NO₂⁻ are detected in the degradation solution at different times (as seen in Figure 9). The concentration of NO₂⁻ was very low, and the highest concentration of NO₂⁻ was reached in the reaction at 2 h. However, the concentration of NO₃⁻ enhances with the reaction. The amino group should be converted to NO₂⁻, then to NO₃⁻ ($-\text{NH}_2 \rightarrow \text{NO}_2^- \rightarrow \text{NO}_3^-$).

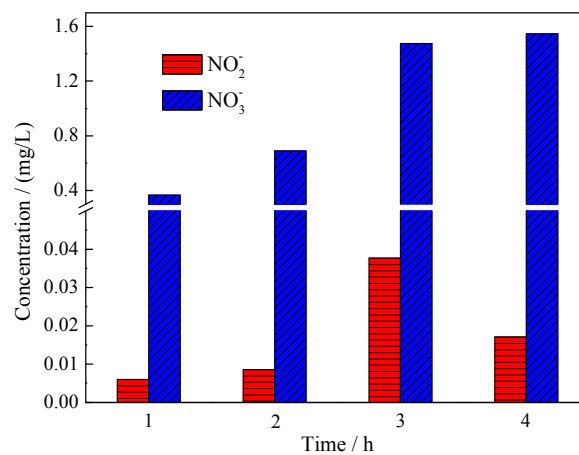


Figure 9. Changes in NO_3^- and NO_2^- concentrations in the photocatalytic degradation of benzohydroxamic acid by 0.50% Yb/TiO₂.

3.4. Calculations and Interfacial Charge Transfer Processes

The calculated band structure of anatase TiO₂ (unit cell) exhibits an indirect band gap of 2.105 eV (Figure 10), which is lower than the experimental values, but the electronic structure is otherwise essentially the same [35]. For the doped structure, a supercell of $2 \times 2 \times 1$ 48-atom anatase TiO₂ was used, and one Ti atom near the centre of the supercell was replaced by one Yb atom. The calculated band structure of doped TiO₂ is 2.029 eV, which is lower than for pure TiO₂, and is consistent with the experimental results in this study.

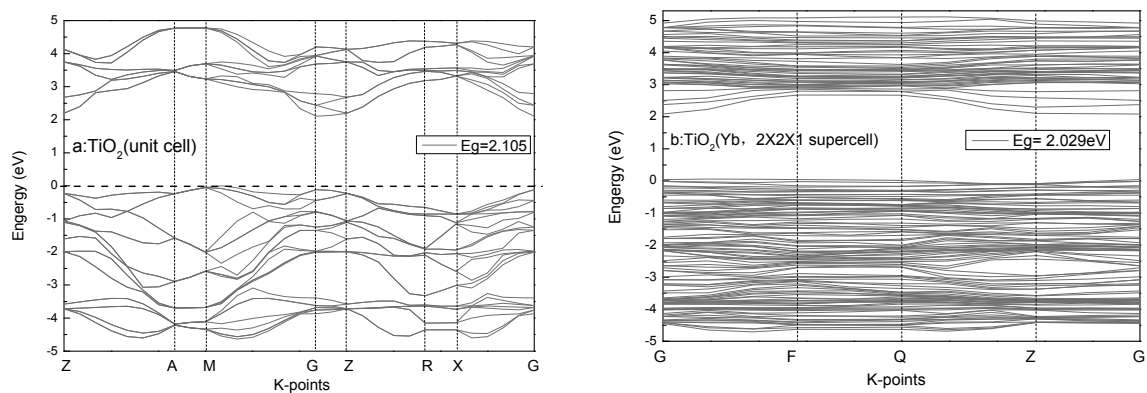


Figure 10. Band-gap structures of pure anatase TiO₂ and Yb-doped anatase TiO₂ ($2 \times 2 \times 1$ supercell).

It is clear from the screening plots (Figure 11) that the introduced Yb 4f orbital mainly contributes to the top of the valence band, extending the impurities' energy level into the forbidden band and producing a wider valence band in comparison with the pure cases. Meanwhile, both the top of the valence band and the bottom of the conduction band shift slightly with respect to the Fermi level, which results in the band gap narrowing and the consequent redshift response of the optical absorption edge.

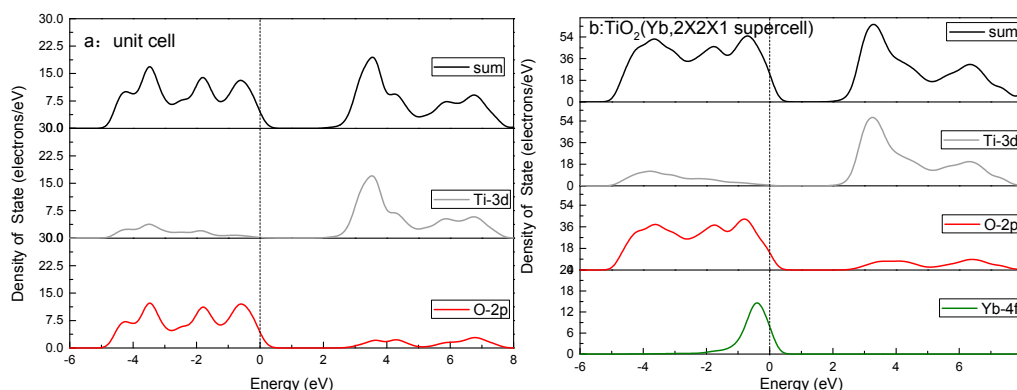
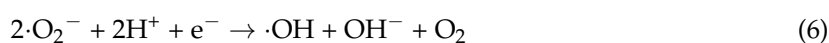


Figure 11. The calculated density of states of pure TiO₂ and Yb-doped TiO₂ (2 × 2 × 1 supercell).

The photocatalytic mechanism of Yb/TiO₂ may be related to the 4f electronic structure of Yb and its variable valences (+2, +3). Yb³⁺ in Yb/TiO₂ trapped the photoexcited electrons to translate to Yb²⁺. Yb²⁺ was translated to Yb³⁺ again by release of an electron, and the released electron could be easily captured by O₂ adsorbed on the surface of TiO₂ to produce ·O₂[−] [9]. On one hand, the process above could inhibit the recombination of photoinduced charge (Equations (4)–(6)); on the other hand, the produced ·O₂[−] could enhance the oxidation of BHA (Equation (7)).



4. Conclusions

Yb/TiO₂ composites were prepared, characterized, and calculated by computer. Compared with pure TiO₂, the XRD diffraction peaks of Yb/TiO₂ were weaker and broader. The composition doped with Yb could suppress grain growth, enhance the thermal stability of anatase, and increase the S_{BET} of TiO₂. Yb/TiO₂ also had lower gap energy and more regular shape in morphology than pure TiO₂. In addition, 0.50% Yb/TiO₂ (450 °C) indicated higher photocatalytic degradation ability with respect to BHA: the degradation efficiency and mineralization rate of BHA reached 95.5% and 89.2%, respectively, after 120 min with 300 W mercury. The doped Yb could promote the separation of photo-excited electrons and holes, resulting in the increase of the degradation rate of BHA. Moreover, ·OH was the main active species during the photocatalytic process, and NO₃[−] was the dominant product of the amino group.

Supplementary Materials: The following are available online at www.mdpi.com/1660-4601/14/12/1471/s1, Figure S1: The unit cell of anatase TiO₂ (a) and a Yb-doped anatase TiO₂ supercell (b). The red, gray, and green spheres represent oxygen, titanium, and Ytterbium atoms, respectively; Figure S2: EDS of Yb/TiO₂ (a). Element mapping images of Ti (b), O (c), and Yb (d) of Yb/TiO₂; Figure S3: Effect of different calcination temperatures on photocatalytic degradation of benzohydroxamic acid (BHA). The BHA concentration was 30 mg/L, and the catalyst dosage was 0.3 g/L; Figure S4: Recycle tests of Yb/TiO₂. The BHA concentration was 30 mg/L, and the catalyst dosage was 0.5 g/L; Figure S5: TOC efficiency by 0.50% Yb/TiO₂, pure TiO₂, and blank. The BHA concentration was 30 mg/L, and the catalyst dosage was 0.3 g/L.

Acknowledgments: The study was supported by National Natural Science Foundation of China (51408277, 21607064); China's Postdoctoral Science Fund (2016T90967, 2015M582776XE); the Program of 5511 Talents in Scientific and Technological Innovation of Jiangxi Province (20165BCB18014), and the Program of Qingjiang Excellent Young Talents, Jiangxi University of Science and Technology.

Author Contributions: Chunying Wang presented the original idea for the study. Junyu Wang and Sipin Zhu carried out the experiment, analyzed the data, and drafted the manuscript. Xianping Luo, Chunying Wang and Min Wu conducted the discussion, interpreted the data and modified the manuscript. All authors have read the manuscript and agreed to submission.

Conflicts of Interest: The authors declare no conflict of interest.

References

1. Lyu, J.; Gao, J.; Zhang, M.; Fu, Q.; Sun, L.; Hu, S.; Zhong, J.; Wang, S.; Li, J. Construction of homojunction-adsorption layer on anatase TiO₂ to improve photocatalytic mineralization of volatile organic compounds. *Appl. Catal.* **2017**, *202*, 664–670. [[CrossRef](#)]
2. Salasbañales, E.; Quirozsegoviano, R.I.; Díazalejo, L.A.; Rojasgonzález, F.; Estrellagonzález, A.; Campero, A.; Garcíasánchez, M.A. Comparative study of the optical and textural properties of tetrapyrrole macrocycles trapped within ZrO₂, TiO₂, and SiO₂ translucent xerogels. *Molecules* **2015**, *20*, 19463–19488. [[CrossRef](#)] [[PubMed](#)]
3. He, D.; Huang, X.; Zhao, S.; Hu, D. Synthesis and catalytic performance of Yb³⁺, Er³⁺ doped titanium dioxide. *Asian J. Chem.* **2015**, *27*, 1477–1480. [[CrossRef](#)]
4. Saqib, N.U.; Adnan, R.; Shah, I. A mini-review on rare earth metal-doped TiO₂ for photocatalytic remediation of wastewater. *Environ. Sci. Pollut. Res.* **2016**, *23*, 15941. [[CrossRef](#)] [[PubMed](#)]
5. Xu, W.-W.; Dai, S.-Y.; Hu, L.-H.; Liang, L.-Y.; Wang, K.-J. Influence of Yb-doped nanoporous TiO₂ films on photovoltaic performance of dye-sensitized solar cells. *Chin. Phys. Lett.* **2006**, *23*, 2288–2291.
6. Qu, X.; Yan, X.; Hou, Y.; Wang, P.; Song, H.; Du, F. Preparation of Gd-doped TiO₂ hollow spheres with enhanced photocatalytic performance. *J. Sol-Gel Sci. Technol.* **2015**, *76*, 699–707. [[CrossRef](#)]
7. Reszczyńska, J.; Grzyb, T.; Sobczak, J.W.; Lisowski, W.; Gazda, M.; Ohtani, B.; Zaleska, A. Visible light activity of rare earth metal doped (Er³⁺, Yb³⁺ or Er³⁺ /Yb³⁺) titania photocatalysts. *Appl. Catal.* **2015**, *163*, 40–49. [[CrossRef](#)]
8. Devi, L.G.; Kumar, S.G. Exploring the critical dependence of adsorption of various dyes on the degradation rate using Ln³⁺-TiO₂ surface under UV/solar light. *Appl. Surf. Sci.* **2012**, *261*, 137–146. [[CrossRef](#)]
9. Samadi, M.; Zirak, M.; Naseri, A.; Khorashadizade, E.; Moshfegh, A.Z. Recent progress on doped ZnO nanostructures for visible-light photocatalysis. *Thin Solid Films* **2016**, *605*, 2–19. [[CrossRef](#)]
10. Sun, L.; Hu, Y.-H.; Sun, W. Effect and mechanism of octanol in cassiterite flotation using benzohydroxamic acid as collector. *Trans. Nonferrous Met. Soc. China* **2016**, *26*, 3253–3257. [[CrossRef](#)]
11. Hashimoto, S.; Nakamura, Y. Nuclease activity of a hydroxamic acid derivative in the presence of various metal ions. *J. Chem. Soc. Chem. Commun.* **1995**, *14*, 1413–1414. [[CrossRef](#)]
12. Wenjun, Z. Study on the Biodegradability of Hydroxamic Acid Collectors. Ph.D. Thesis, Wuhan University of Technology, Wuhan, China, 2012.
13. Luo, X.; Wang, J.; Wang, C.; Zhu, S.; Li, Z.; Tang, X.; Wu, M. Degradation and mineralization of benzohydroxamic acid by synthesized mesoporous La/TiO₂. *Int. J. Environ. Res. Public Health* **2016**, *13*, 997. [[CrossRef](#)] [[PubMed](#)]
14. Fidelus, J.D.; Barczak, M.; Michalak, K.; Fekner, Z.; Dużyńska, A.; Jusza, A.; Pyramidowicz, R.; Monty, C.J.; Suchocki, A. Microstructural and optical characterization of TiO₂ doped with ytterbium synthesized by sol-gel and solar physical vapor deposition process. *J. Nanosci. Nanotechnol.* **2012**, *12*, 3760–3765. [[CrossRef](#)] [[PubMed](#)]
15. Calandra, P.; Lombardo, D.; Pistone, A.; Liveri, V.T.; Trusso, S. Structural and optical properties of novel surfactant-coated Yb@TiO₂ nanoparticles. *J. Nanopart. Res.* **2011**, *13*, 5833–5839. [[CrossRef](#)]
16. Clark Stewart, J.; Segall Matthew, D.; Pickard Chris, J.; Hasnip Phil, J.; Probert Matt, I.J.; Refson, K.; Payne Mike, C. First principles methods using CASTEP. *J. Crystallogr. Cryst. Mater.* **2005**, *220*, 567–570.
17. Khalid, N.R.; Ahmed, E.; Rasheed, A.; Ahmad, M.; Ramzan, M.; Shakoob, A.; Elahi, A.; Abbas, S.M.; Hussain, R.; Niaz, N.A. Co-doping effect of carbon and yttrium on photocatalytic activity of TiO₂ nanoparticles for methyl orange degradation. *J. Ovonic Res.* **2015**, *11*, 107–112.
18. Fan, W.Q.; Bai, H.Y.; Zhang, G.H.; Yan, Y.S.; Liu, C.B.; Shi, W.D. Titanium dioxide macroporous materials doped with iron: Synthesis and photo-catalytic properties. *Crystengcomm* **2013**, *16*, 116–122. [[CrossRef](#)]

19. Liu, H.; Yu, L.; Chen, W.; Li, Y. The progress of TiO₂ nanocrystals doped with rare earth ions. *J. Nanomater.* **2012**, *2012*, 1–9.
20. Wang, J.; Yang, G.; Wang, L.; Yan, W. Fabrication of a well-aligned TiO₂ nanofibrous membrane by modified parallel electrode configuration with enhanced photocatalytic performance. *RSC Adv.* **2016**, *6*, 31476–31483. [[CrossRef](#)]
21. Spadavecchia, F.; Cappelletti, G.; Ardizzone, S.; Bianchi, C.L.; Cappelli, S.; Oliva, C.; Scardi, P.; Leoni, M.; Fermo, P. Solar photoactivity of nano-N-TiO₂ from tertiary amine: role of defects and paramagnetic species. *Appl. Catal.* **2010**, *96*, 314–322. [[CrossRef](#)]
22. Liew, S.L.; Zhang, Z.; Goh, T.W.G.; Subramanian, G.S.; Seng, H.L.D.; Hor, T.S.A.; Luo, H.K.; Chi, D.Z. Yb-doped WO₃ photocatalysts for water oxidation with visible light. *Int. J. Hydrog. Energy* **2014**, *39*, 4291–4298. [[CrossRef](#)]
23. Huang, F.; Guo, Y.; Wang, S.; Zhang, S.; Cui, M. Solgel-hydrothermal synthesis of Tb/Tourmaline/TiO₂ nano tubes and enhanced photocatalytic activity. *Solid State Sci.* **2017**, *64*, 62–68. [[CrossRef](#)]
24. Wu, X.; Fang, S.; Zheng, Y.; Sun, J.; Lv, K. Thiourea-modified TiO₂ nanorods with enhanced photocatalytic activity. *Molecules* **2016**, *21*, 181. [[CrossRef](#)] [[PubMed](#)]
25. Das, S.K.; Bhunia, M.K.; Sinha, A.K.; Bhaumik, A. Synthesis, characterization, and biofuel application of mesoporous zirconium oxophosphates. *ACS Catal.* **2011**, *1*, 493–501. [[CrossRef](#)]
26. Li, X.; Lin, H.; Chen, X.; Niu, H.; Zhang, T.; Liu, J.; Qu, F. Fabrication of TiO₂/porous carbon nanofibers with superior visible photocatalytic activity. *New J. Chem.* **2015**, *39*, 7863–7872. [[CrossRef](#)]
27. Reszczynska, J.; Grzyb, T.; Wei, Z.; Klein, M.; Kowalska, E.; Ohtani, B.; Zaleska-Medynska, A. Photocatalytic activity and luminescence properties of RE³⁺-TiO₂ nanocrystals prepared by sol-gel and hydrothermal methods. *Appl. Catal.* **2016**, *181*, 825–837. [[CrossRef](#)]
28. Trujillo-Navarrete, B.; María del Pilar, H.-V.; Rosa María, F.-N.; Francisco, P.-D.; Henry, A.-H.; Sergio, P.-S.; Edgar Alonso, R.-S. Effect of Nd³⁺ doping on structure, microstructure, lattice distortion and electronic properties of TiO₂ nanoparticles. *J. Rare Earths* **2017**, *35*, 259–270. [[CrossRef](#)]
29. Hu, C.; Yu, J.C.; Hao, Z.; Wong, P.K. Effects of acidity and inorganic ions on the photocatalytic degradation of different azo dyes. *Appl. Catal.* **2003**, *46*, 35–47. [[CrossRef](#)]
30. Sörensen, M.; Frimmel, F.H. Photochemical degradation of hydrophilic xenobiotics in the ja:math process: Influence of nitrate on the degradation rate of EDTA, 2-amino-1-naphthalenesulfonate, diphenyl-4-sulfonate and 4,4'-diaminostilbene-2,2'-disulfonate. *Acta Hydroch. Hydrob.* **1997**, *31*, 2885–2891.
31. Dong, H.K.; Anderson, M.A. Solution factors affecting the photocatalytic and photoelectrocatalytic degradation of formic acid using supported TiO₂ thin films. *J. Photochem. Photobiol. A* **1996**, *94*, 221–229.
32. Wang, C.; Zhu, L.; Wei, M.; Chen, P.; Shan, G. Photolytic reaction mechanism and impacts of coexisting substances on photodegradation of bisphenol A by Bi₂WO₆ in water. *Water Res.* **2012**, *46*, 845–853. [[CrossRef](#)] [[PubMed](#)]
33. Giraldo, A.L.; Penuela, G.A.; Torres-Palma, R.A.; Pino, N.J.; Palominos, R.A.; Mansilla, H.D. Degradation of the antibiotic oxolinic acid by photocatalysis with TiO₂ in suspension. *Water Res.* **2010**, *44*, 5158–5167. [[CrossRef](#)] [[PubMed](#)]
34. Liu, S.Q.; Yang, M.Q.; Zhang, N.; Xu, Y.J. Nanocomposites of graphene-CdS as photoactive and reusable catalysts for visible-light-induced selective reduction process. *J. Energy Chem.* **2014**, *23*, 145–155. [[CrossRef](#)]
35. Wei, Z.-N.; Jia, C.-L. First-principle calculations of the electronic and optical properties of Tm-doped anatase titanium dioxide. *Opt. Eng.* **2015**. [[CrossRef](#)]

